Check for updates

Received: 31 August 2023 | Revised: 20 December 2023 | Accepted: 3 January 2024

DOI: 10.1002/cey2.556

RESEARCH ARTICLE

CARBON ENERGY WILEY

Activating Ru in the pyramidal sites of Ru_2P-type structures with earth-abundant transition metals for achieving extremely high HER activity while minimizing noble metal content

Sayed M. El-Refaei[1,2] | **Patrícia A. Russo**[1] | **Thorsten Schultz**[3,4] | **Zhe-Ning Chen**[5] | **Patrick Amsalem**[3] | **Norbert Koch**[3,4] | **Nicola Pinna**[1]

[1]Department of Chemistry and the Center for the Science of Materials Berlin, Humboldt-Universität zu Berlin, Berlin, Germany

[2]Max-Planck-Institut für Chemische Energiekonversion, Mülheim an der Ruhr, Germany

[3]Institut für Physik and Center for the Science of Materials Berlin, Humboldt-Universität zu Berlin, Berlin, Germany

[4]Helmholtz-Zentrum Berlin für Materialien und Energie GmbH, Berlin, Germany

[5]State Key Laboratory of Structural Chemistry, Fujian Institute of Research on the Structure of Matter, Chinese Academy of Sciences, Fuzhou, China

Correspondence

Patrícia A. Russo and Nicola Pinna, Department of Chemistry and the Center for the Science of Materials Berlin, Humboldt-Universität zu Berlin, Brook-Taylor-Straße 2, 12489 Berlin, Germany.
Email: patricia.russo@hu-berlin.de and nicola.pinna@hu-berlin.de

Funding information

National Natural Science Foundation of China, Grant/Award Number: 22173105

Abstract

Rational design of efficient pH-universal hydrogen evolution reaction catalysts to enable large-scale hydrogen production via electrochemical water splitting is of great significance, yet a challenging task. Herein, Ru atoms in the Ru_2P structure were replaced with M = Co, Ni, or Mo to produce $M_{2-x}Ru_xP$ nanocrystals. The metals show strong site preference, with Co and Ni occupying the tetrahedral sites and Ru the square pyramidal sites of the CoRuP and NiRuP Ru_2P-type structures. The presence of Co or Ni in the tetrahedral sites leads to charge redistribution for Ru and, according to density functional theory calculations, a significant increase in the Ru d-band centers. As a result, the intrinsic activity of CoRuP and NiRuP increases considerably compared to Ru_2P in both acidic and alkaline media. The effect is not observed for MoRuP, in which Mo prefers to occupy the pyramidal sites. In particular, CoRuP shows state-of-the-art activity, outperforming Ru_2P with Pt-like activity in 0.5 M H_2SO_4 ($\eta_{10} = 12.3$ mV; $\eta_{100} = 52$ mV; turnover frequency (TOF) = 4.7 s^{-1}). It remains extraordinarily active in alkaline conditions ($\eta_{10} = 12.9$ mV; $\eta_{100} = 43.5$ mV) with a TOF of 4.5 s^{-1}, which is 4x higher than that of Ru_2P and 10x that of Pt/C. Further increase in the Co content does not lead to drastic loss of activity, especially in alkaline medium, where, for example, the TOF of $Co_{1.9}Ru_{0.1}P$ remains comparable to that of Ru_2P and higher than that of Pt/C, highlighting the viability of the adopted approach to prepare cost-efficient catalysts.

KEYWORDS

electrocatalysis, ruthenium phosphide, transition metal phosphonates

This is an open access article under the terms of the Creative Commons Attribution License, which permits use, distribution and reproduction in any medium, provided the original work is properly cited.
© 2024 The Authors. *Carbon Energy* published by Wenzhou University and John Wiley & Sons Australia, Ltd.

1 | INTRODUCTION

Water electrolysis, when powered by electricity generated from renewable sources, is considered to be a sustainable technology to produce green hydrogen (H_2), which is an energy carrier with a high energy density that could potentially replace fossil fuels.[1–3] Electrocatalysts are required to promote the hydrogen evolution reaction (HER) at suitable rates over a broad pH range, to achieve commercial large-scale H_2 production via water electrolysis.[2,4] Platinum is the most efficient catalyst for HER in acidic medium.[4] However, its prohibitively high price has led to extensive research over the last decade for developing effective but cheaper catalysts based on Earth-abundant transition metals.[4] Transition-metal phosphides were found to be among the most promising catalytic materials for acidic HER.[4,5] However, producing H_2 at high rates in alkaline solutions remains a challenge, as even the activity of Pt decreases by 2–3 orders of magnitude compared to that in acidic media, owing to the high kinetic energy barrier for the water dissociation that slows down the overall reaction.[4–6] Therefore, developing active, durable, and economically viable materials to catalyze the HER in acidic as well as alkaline environments is crucial for the implementation of a future H_2-based economy.

Recent studies indicate that Ru-based catalysts are suitable candidates for the HER in a broad pH range. Ru has moderate hydrogen-bond strength, comparable to that of Pt (62 kcal mol^{-1} for Ru–H and 65 kcal mol^{-1} for Pt–H),[4,7,8] higher corrosion resistance, smaller water dissociation barrier than Pt, and is also significantly less expensive, making it promising for both acidic and alkaline water electrolyzers.[9] Nevertheless, research on Ru-based catalysts is still in its early stages.[10] It has been mainly focused on attempting to achieve high activity while further decreasing the catalysts' costs. In addition, the performance of many of the Ru-based materials remains inferior to that of commercial Pt/C, particularly in acidic media.

Alloying Ru with Earth-abundant transition metals (e.g., Fe, Co, Ni, Cu, Mo, etc.) allows to tune the electronic properties and thus enhance the HER performance while simultaneously mitigating the costs.[11] For instance, Lu et al.[8] reported bimetallic RuNi nanoparticles anchored on carbon quantum dots (RuNi/CQDs) exhibiting outstanding performance (overpotentials at $-10\,mA\,cm^{-2}$ are 13, 58, and 18 mV in 1.0 M KOH, 0.5 M H_2SO_4, and 1.0 M phosphate buffer solution, respectively) over a wide pH range. The authors suggested that alloying Ru with Ni optimized the H-binding energy nearby the surface Ru atoms. Likewise, RuCo[12,13] and RuMo[14] alloys showed potential to increase the Ru activity while decreasing the catalyst cost.

The combination of Ru with nonmetals such as P in phosphide compounds has also been investigated in this context with promising results. Ru phosphides can adopt four structures depending on the Ru/P ratio (Ru_2P, RuP, RuP_2, and RuP_4).[15,16] The importance of the phosphide phase on the HER activity in acidic medium was studied by Liu et al.,[15] who reported that the intrinsic activity increases with increasing the Ru/P ratio of the structure ($Ru_2P > RuP > RuP_2$). Similarly, Kim et al.[17] reported that Ru phosphides with a higher Ru/P ratio exhibit higher HER activity in alkaline conditions, possibly due to a higher degree of hydroxylated Ru species on their surface that facilitates water dissociation during the Volmer step.

Further dilution of the Ru with Earth-abundant transition metals in bimetallic Ru phosphides is expected to enable additional tuning of the electronic properties to reach high performances. Indeed, amorphous RuCoP clusters fabricated by direct phosphorization of pre-synthesized RuCo alloy exhibited excellent HER performance in acidic as well as in alkaline media, outperforming Ru and Ru/CoP clusters.[18] Similarly, amorphous RuFeP nanoclusters supported on carbon nanofibers showed high activity, requiring small overpotentials of 65.8 and 16 mV to reach a current density of $-10\,mA\,cm^{-2}$ in acidic and alkaline media, respectively.[19] Despite such results, bimetallic Ru phosphides have been scarcely studied until now. Part of the reason may be the difficulty in producing $M_xRu_yP_z$ with well-defined and controlled structures under mild synthesis conditions because combining two metals homogenously in the same phosphide crystal structure is a complex task due to the tendency for multiple phase formation caused by the different phosphide structures in which different metals crystallize.[5] In fact, the studies reported so far comprise catalysts that are amorphous or have very low crystallinity and mixtures of different single-metal compounds and/or phases, where solid solutions are not formed.[18,19] These types of catalysts can lead to outstanding performance due to factors like high defect contents and high amounts of exposed active sites, as well as doping and interfacing, which can modulate the electronic properties. However, investigating specific and well-defined bimetallic phosphide structures is also important to establishing clear relationships between structure, composition, and activity.

Herein, we report the high HER activity in both acidic and alkaline environments of $M_{2-x}Ru_xP$ nanocrystalline catalysts (M = Mo, Ni, Co) adopting the same orthorhombic crystal structure as Ru_2P. To the best of our knowledge, it is the first time that such structures are

26379368, 2024, 9, Downloaded from https://onlinelibrary.wiley.com/doi/10.1002/cey2.556 by Humboldt-Universitat Zu Berlin, Wiley Online Library on [06/01/2025]. See the Terms and Conditions (https://onlinelibrary.wiley.com/terms-and-conditions) on Wiley Online Library for rules of use; OA articles are governed by the applicable Creative Commons License

investigated as HER electrocatalysts. Bulk MoRuP,[20] NiRuP,[21] and CoRuP[21] have been synthesized before, although under harsh conditions such as high temperatures and pressures. The bimetallic phases, particularly CoRuP and NiRuP, are highly active in acidic and alkaline media, despite the decrease in noble metal content. To drive current densities of −10 and −100 mA cm^{-2} in 0.5 M H_2SO_4, CoRuP, NiRuP, and MoRuP require overpotentials of 12.3, 14.2, and 30.4 mV and 52.0, 60.8, and 77.9 mV, respectively. The values in 1.0 M KOH are 12.9, 16.0, and 23.7 mV at −10 mA cm^{-2} and 43.5, 68.7, and 77.6 mV at −100 mA cm^{-2}, respectively. The preparation of nanocrystalline solid solutions allowed the establishment of correlations between the activity and the structure of the metal sites.

2 | RESULTS AND DISCUSSION

The carbon-embedded $M_{2-x}Ru_xP$ nanocrystals (M = Co, Ni, Mo) with different Ru contents were synthesized via thermal decomposition of M,Ru-carboxyphosphonates. In the first step, M,Ru-(phosphonomethyl)iminodiacetate compounds with the desired metal composition were synthesized to act as single-source precursors of the M,Ru phosphides. The precursors provide all the necessary elements (metals, phosphorus, and carbon) for the final products with a homogeneous distribution.[22] In the second step, the precursors were converted to metal phosphides by pyrolysis under Ar/H_2(5%) atmosphere. The target products were bimetallic phosphides with Ru_2P-type structures. Among the pure Ru phosphides, the phase with the highest metal/P ratio is reportedly the most active for HER in both acidic and alkaline solutions, but its bimetallic analogue nanocrystals have not yet been investigated.[15,17] It was shown before that the metal/P ratio and structure of the final phosphide can be controlled by rational selection of the ligand used to build the precursor.[23] Therefore, the (phosphonomethyl)iminodiacetate ligand was selected to produce the single-source precursors that direct the synthesis toward the formation of the Ru_2P-type structures.

In the first part of this study, we synthesized $M_{2-x}Ru_xP$ catalysts with $x = 1$, that is, with half of the Ru atoms in the structure replaced with Co, Ni, or Mo, and evaluated them as HER electrocatalysts in acidic and alkaline media. Figure 1A shows that all the synthesized catalysts adopt the targeted orthorhombic Ru_2P-type structure without any other crystalline phases being present in the X-ray diffraction (XRD) patterns. The broadened diffractions suggest the formation of small crystallites and nanocrystals. Importantly, the diffraction peaks shift to lower or higher angles with respect to Ru_2P, depending on the size of the second metal, suggesting the formation of true solid solutions with orthorhombic Ru_2P-type structures containing the two metals.[20] Thus, Ni and Co, which are smaller than Ru, according to the general atomic radii trend in the periodic table, cause shifts to higher 2θ angles, while the peaks are slightly shifted in the opposite direction for MoRuP due to the larger size of Mo compared to Ru.

Transmission electron microscopy (TEM) reveals the formation of small nanocrystals surrounded by a carbon

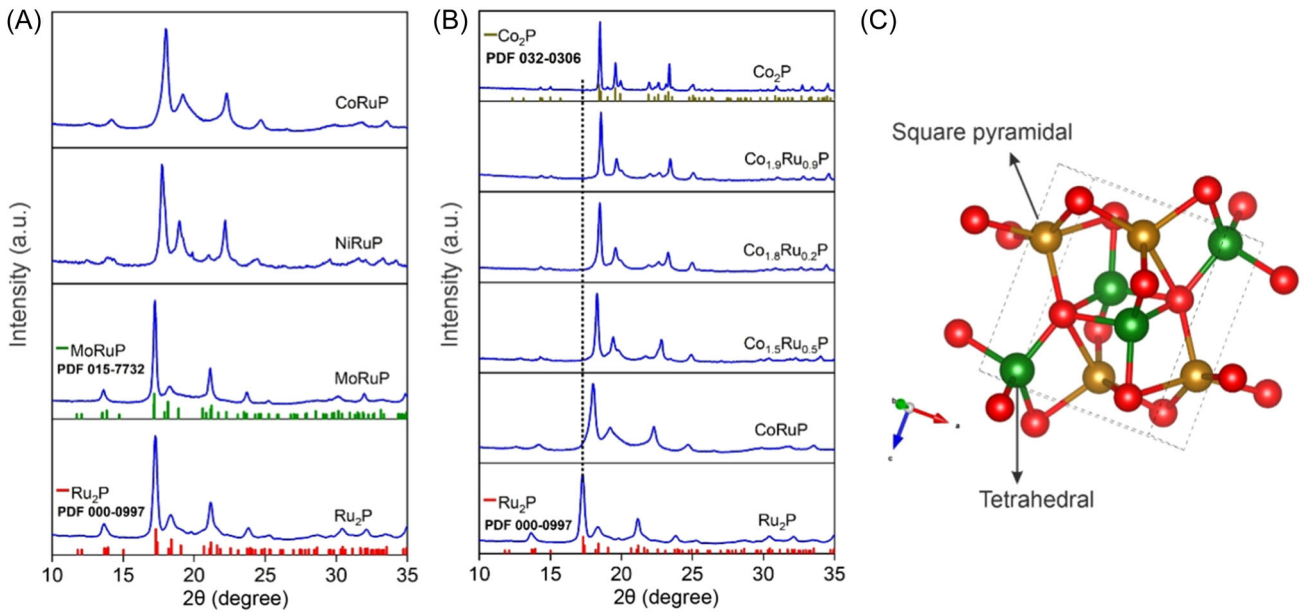

FIGURE 1 (A, B) X-ray diffractograms of the $M_{2-x}Ru_xP$ catalysts. (C) Ru_2P structure, showing the tetrahedral and square pyramidal metal sites. Vertical lines represent ICDD PDF files (Ru_2P- PDF 000-0997, MoRuP- PDF 015-7732, and Co_2P- PDF 032-0306).

26379368, 2024, 9, Downloaded from https://onlinelibrary.wiley.com/doi/10.1002/cey2.556 by Humboldt-Universitat Zu Berlin, Wiley Online Library on [06/01/2025]. See the Terms and Conditions (https://onlinelibrary.wiley.com/terms-and-conditions) on Wiley Online Library for rules of use; OA articles are governed by the applicable Creative Commons License

matrix that subsequently forms larger secondary agglomerates, as shown in Figure 2 for CoRuP and Figures S1 and S2 for NiRuP and MoRuP. The small sizes of the nanocrystals explain the peak broadening observed in the XRD patterns, a phenomenon known as Scherrer broadening. Despite their small size, high-resolution TEM (HRTEM) shows that the particles are very well crystallized. Further analysis of individual CoRuP nanocrystals gives a calculated interplanar spacing of 0.225 nm that can be ascribed to the (112) planes of the orthorhombic CoRuP lattice. The selected area electron diffraction pattern (SAED) is indexed to the orthorhombic structure of CoRuP, further corroborating the XRD analysis (Figure 2B, inset). The (phosphonomethyl) iminodiacetate ligand decomposition during the pyrolysis step induced the formation of a carbon shell encapsulating the phosphide core (as indicated by the red arrows in Figure 2B and Figure S1), which shows lattice fringes on the carbon layer with d spacing of ca. 0.335 nm, consistent with the d_{002} of graphite. This phenomenon is discussed in detail in our previous publication, where the same ligand was employed to promote the formation of orthorhombic CoMoP.[23] The presence of two carboxylate groups in the ligand renders low thermal stability that is responsible for the formation of agglomerates surrounded by a thin carbon shell at low pyrolysis temperature.[23] The carbon shell is believed to increase the conductivity of the catalysts and thus facilitate the charge transfer reaction as well as enhance the stability, as discussed in previous studies.[22,23] High-angle annular dark field-scanning transmission electron microscopy (HAADF-STEM) imaging reveals the porosity of the derived core-shell structure, which is beneficial for electrocatalysis as it increases the accessibility to the active sites. The energy-dispersive X-ray spectroscopy (EDS) elemental maps confirm that Ru, Co, and P are homogenously distributed throughout the RuCoP structure (Figure 2C). Element quantification gives Ru:Co:P ratios of ca. 1:1:1, in agreement with the expected composition (Table S1). Inductively coupled plasma optical emission spectroscopy (ICP-OES) measurements were performed to further check the elemental ratios. The data (Table S2) corroborate the EDS findings. The results are analogous for NiRuP and MoRuP in terms of morphological and microstructure properties, as well as element distribution and M:Ru:P ratios (Figures S2 and S3). These results provide further evidence of the formation of MRuP crystals comprising the two metals in Ru_2P-type structures and the absence of metal segregation.

The HER activity of the catalysts was investigated in 0.5 M H_2SO_4 and 1.0 M KOH solutions (Figure 3). The measurements were performed on glassy carbon (GC) electrodes, with mass loadings of 0.25 mg cm^{-2} for all the catalysts. Commercial Pt/C (20 wt%) was used to benchmark

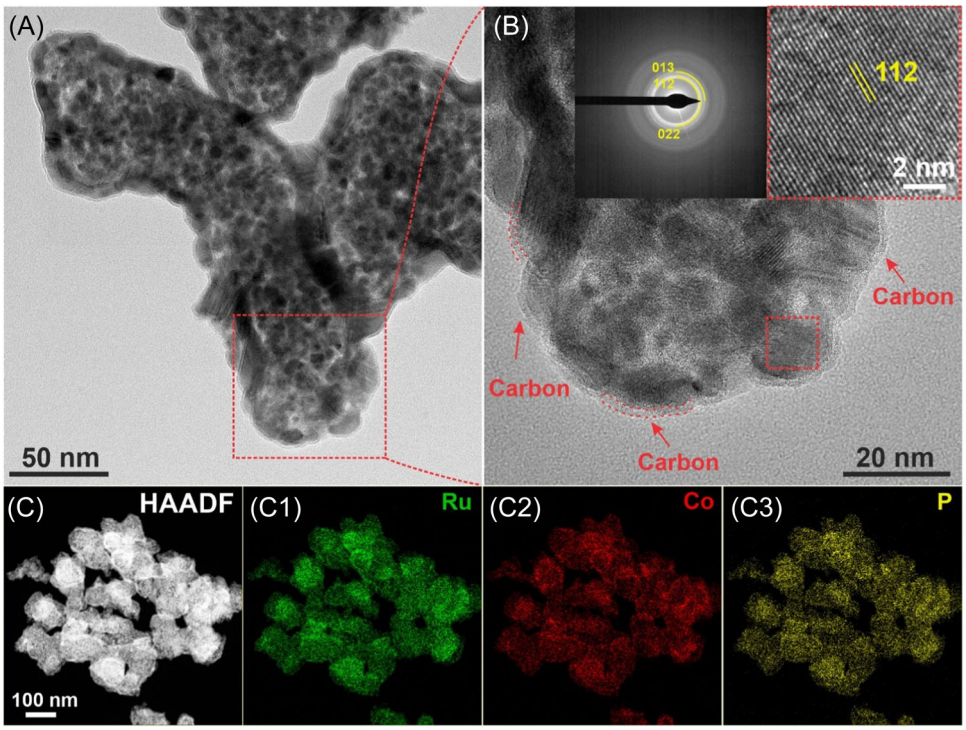

FIGURE 2 (A) TEM, (B) HRTEM of CoRuP (inset SAED pattern), and (C and C1–3) HAADF-STEM images and corresponding EDS maps of Ru, Co, and P.

26379368, 2024, 9, Downloaded from https://onlinelibrary.wiley.com/doi/10.1002/cey2.556 by Humboldt-Universitat Zu Berlin, Wiley Online Library on [06/01/2025]. See the Terms and Conditions (https://onlinelibrary.wiley.com/terms-and-conditions) on Wiley Online Library for rules of use; OA articles are governed by the applicable Creative Commons License

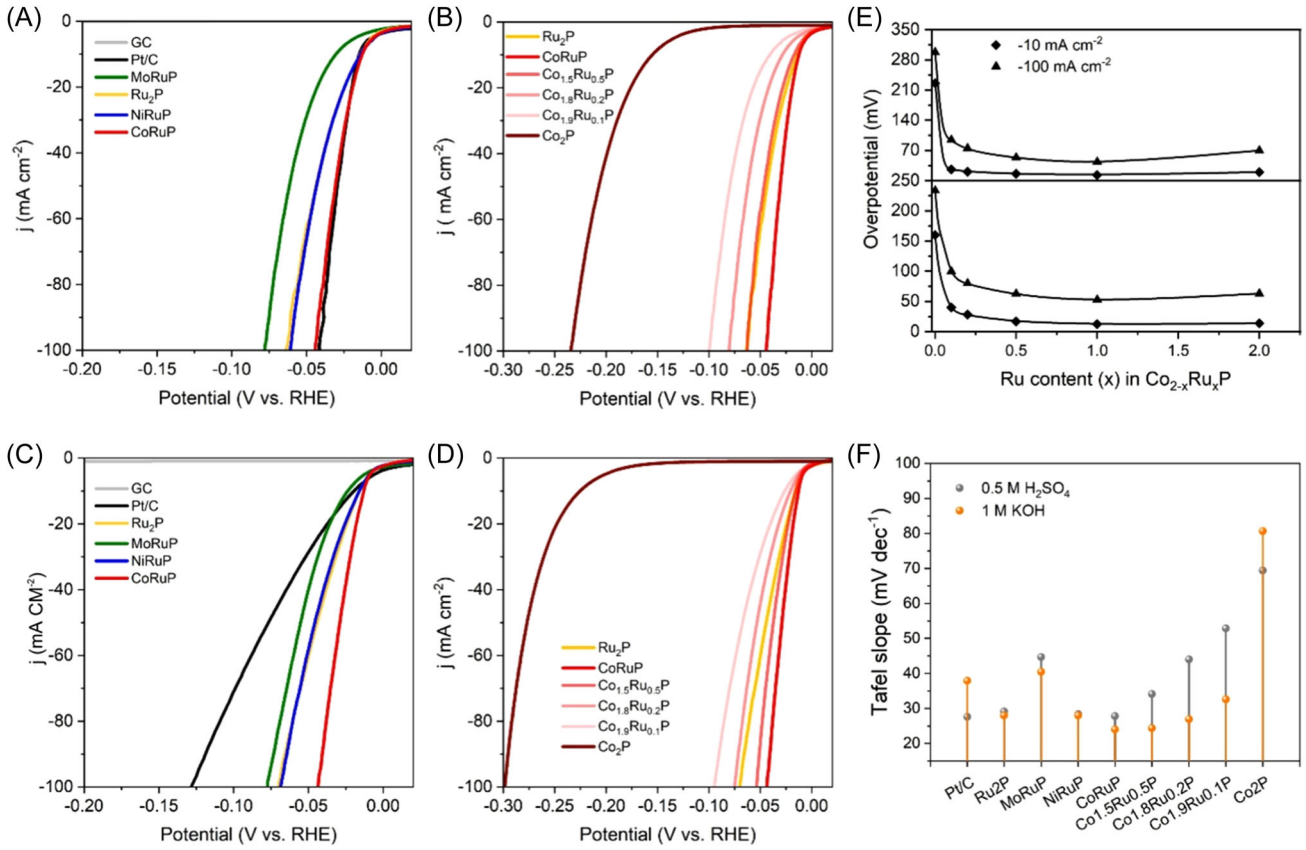

FIGURE 3 HER polarization curves of the $M_{2-x}Ru_xP$ catalysts in (A, B) 0.5 M H_2SO_4 and (C, D) 1.0 M KOH; (E) overpotentials at -10 and -100 mA cm^{-2} for the $Co_{2-x}Ru_xP$ catalysts, as a function of the Ru content; (F) Tafel slopes.

the HER activity (Figure 3). Its performance agrees with the results published in the literature. Pt/C is extremely active in 0.5 M H_2SO_4, but the activity drastically decreases in 1.0 M KOH, with the overpotential at -10 mA cm^{-2} (η_{10}) increasing by more than threefold and the Tafel slope increasing as well. The activity decrease is attributed to the inability of Pt to promote the dissociation of water molecules at a high rate during the Volmer step, which slows down the overall reaction.

Despite being highly active in acidic solution, Ru_2P still underperforms compared to Pt/C. In alkaline solution, on the contrary, Ru_2P shows $\eta_{10} = 16$ mV and $\eta_{100} = 70$ mV, which are below those of Pt/C. The trend agrees with the electrocatalytic behavior reported for catalysts containing nanocrystalline Ru_2P.[15,24] The replacement of half the Ru atoms in the structure with Co, Ni, or Mo has different effects on the apparent activity of the catalysts. Thus, a performance decline is observed for MoRuP with respect to Ru_2P. NiRuP remains similarly active as Ru_2P, in spite of the 50 at% decrease in Ru content. Finally, Co has the most beneficial effect, enhancing the catalytic activity in both acidic and alkaline solutions. In fact, CoRuP exhibits Pt-like activity in 0.5 M H_2SO_4, with $\eta_{10} = 12.3$ mV and $\eta_{100} = 52$ mV, and remains exceptionally active in 1.0 M KOH, with $\eta_{10} = 12.9$ mV and $\eta_{100} = 43.5$ mV, which makes this catalyst compare favorably with the state-of-the-art catalysts reported in the literature (Table S2).

The Tafel slopes of CoRuP, Ru_2P, and NiRuP in acidic media are close to that of Pt/C (Figure 3F), indicating that the reaction proceeds at very high rates for these catalysts, via a Volmer–Tafel mechanism. The reaction is more sluggish for MoRuP, taking place via a Tafel–Heyrovský mechanism. The reaction kinetics remains very fast in alkaline solution for Ru_2P, CoRuP, and NiRuP, which exhibit Tafel slopes around 30 mV dec^{-1} (Figure 3F). The Tafel analysis confirms the favorable effect of combining Co and Ru for accelerating the HER in both acidic and alkaline environments. The reaction acceleration observed in the basic medium can be ascribed to the dissociation of water molecules being facilitated at the surface of these catalysts due to the oxophilic nature of Co.[25,26] The results suggest that water dissociation is facilitated at the surface of these catalysts and takes place at high rates.

The superior electrocatalytic behavior of CoRuP also becomes evident by comparing the mass activity of the various catalysts. Figure 4A,B shows the mass activity at

26379368, 2024, 9, Downloaded from https://onlinelibrary.wiley.com/doi/10.1002/cey2.556 by Humboldt-Universitat Zu Berlin, Wiley Online Library on [06/01/2025]. See the Terms and Conditions (https://onlinelibrary.wiley.com/terms-and-conditions) on Wiley Online Library for rules of use; OA articles are governed by the applicable Creative Commons License

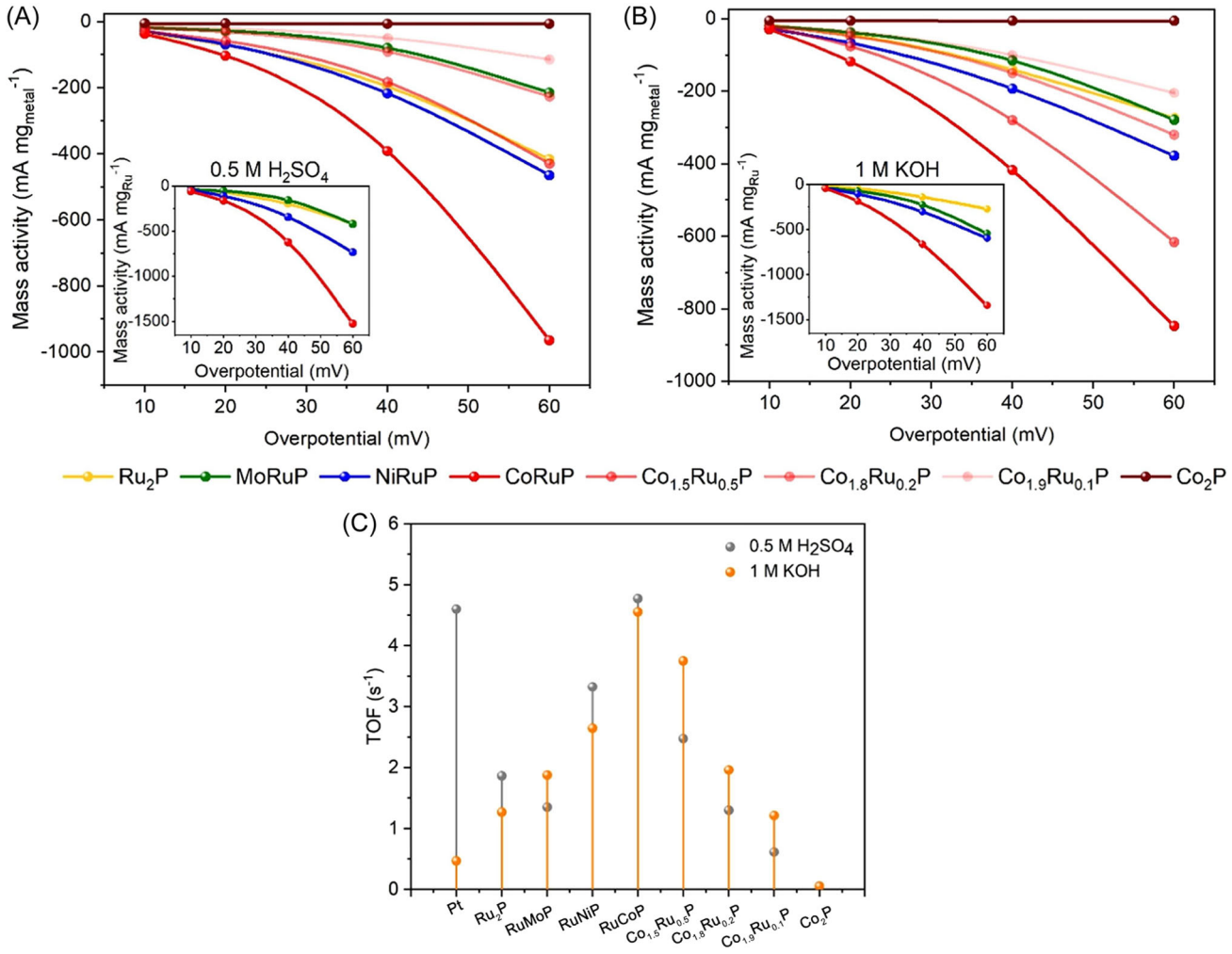

FIGURE 4 Mass activities of the catalysts in (A) 0.5 M H_2SO_4 and (B) 1 M KOH on the basis of the total mass of metal and (insets) mass of Ru in the catalysts; (C) TOF of the catalysts at $\eta = 50$ mV.

different overpotentials in terms of the total mass of metals in the catalyst or the mass of Ru (Figure 4A,B insets). For example, at $\eta = 10$ mV, the HER mass activities of CoRuP are 965 and 848 mA mg_{metal}^{-1} in 0.5 M H_2SO_4 and 1.0 M KOH, respectively, which are significantly higher than those of pure Ru_2P (417 and 273 mA mg_{metal}^{-1}, respectively) and Co_2P (6 mA mg_{metal}^{-1} in both solutions). Additionally, the mass activity in terms of the mass of Ru in the electrodes clearly shows that if the Ru is replaced with Ni or Co and its content is decreased by half, the activity is largely enhanced at both pHs. Thus, the combination of Ru with Ni and, especially, Co in a Ru_2P-type structure may potentially lead to noble-metal-like performances with minimum noble metal content in the electrodes.

The double-layer capacitance (C_{dl}) of the electrodes was also evaluated (Figure S4) due to its relation of proportionality with the electrochemically active surface area (ECSA). Differences in the ECSA can contribute to the differences in the catalytic activity observed. The C_{dl} of all the catalysts is relatively small, as expected, considering that the materials were directly drop-casted onto the GC electrode and not supported on a high surface area support. The C_{dl} values and, thus, the ECSA follow the trend CoRuP > NiRuP > MoRuP, suggesting that CoRuP and NiRuP have more exposed active sites than MoRuP and Ru_2P, which contributes to their higher activity. The differences in ECSA are consistent with the above HRTEM and HAADF analysis, which showed that CoRuP and NiRuP possess porous structures with smaller particles than MoRuP. However, even considering the differences in ECSA, CoRuP, and NiRuP remain more active than Ru_2P, indicating that the differences in performance are associated with the intrinsic activity of the catalysts. The number of active sites can also be inferred from the surface charge, which is derived from cyclic voltammetry (CV) curves measured at pH 7.[18,27] A similar trend is observed in the number of active sites, consistent with the C_{dl} results (Figure S5).

Figure 4C shows the turnover frequency (TOF) values of the catalysts at $\eta = 50$ mV, which gives an estimation

26379368, 2024, 9, Downloaded from https://onlinelibrary.wiley.com/doi/10.1002/cey2.556 by Humboldt-Universitat Zu Berlin, Wiley Online Library on [06/01/2025]. See the Terms and Conditions (https://onlinelibrary.wiley.com/terms-and-conditions) on Wiley Online Library for rules of use; OA articles are governed by the applicable Creative Commons License

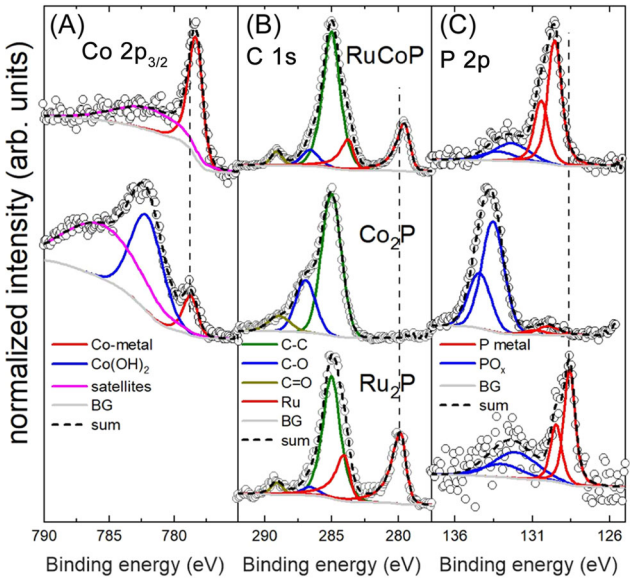

FIGURE 5 High resolution XPS results. (A) Co $2p_{3/2}$, (B) C 1s/Ru 3d, and (C) P 2p spectra of Ru_2P (bottom), Co_2P (middle), and RuCoP (top).

of the intrinsic activity of the active sites. The TOF values of MoRuP, NiRuP, and CoRuP follow the same trend as the apparent and mass activities (CoRuP > NiRuP > MoRuP). MoRuP exhibits slightly smaller TOF than Ru_2P at low pH and similarly at high pH. NiRuP has higher TOF values than Ru_2P in both acidic and alkaline conditions. CoRuP exhibits remarkably high TOF values, identical to that of Pt/C in 0.5 M H_2SO_4 and almost 10 times higher than that of Pt/C and four times higher than that of Ru_2P in 1.0 M KOH. The strong performance of CoRuP and NiRuP can therefore be attributed to the high intrinsic activity of their sites for the HER, originating from the modification of the electronic structure when Co or Ni and Ru are combined.

X-ray photoelectron spectroscopy (XPS) analyses and density functional theory (DFT) calculations were performed to evaluate the electronic alterations occurring when Ru is replaced with Co, Ni, or Mo, and consequently establish the origin of the improved activity. The Co 2p, C 1s/Ru 3d, and P 2p high-resolution spectra of Ru_2P, Co_2P, and RuCoP are shown in Figure 5. The XPS spectra of the other compounds are shown in Figures S6 and S7. Two doublets are observed for all P 2p spectra, one at ~129–130 eV ascribed to metallic phosphide and one at 132.5–134 eV ascribed to oxidized phosphorus species. The Co $2p_{3/2}$ spectrum of Co_2P consists of a small peak at ~779 eV, attributed to metallic cobalt, and a larger peak at ~782.5 eV, attributed to $Co(OH)_2$. In line with the P 2p spectrum, this indicates a strong oxidation of the Co_2P sample during the short air exposure time. The Co $2p_{3/2}$ and P 2p spectra of the CoRuP sample (as well as the other bimetallic samples), on the other hand, show very small oxide peaks, implying a reduced oxidation in the bimetallic compounds. A comparison of the binding energy difference between Ru $3d_{5/2}$ and the metallic P $2p_{3/2}$ component shows a reduction from 151.2 eV for Ru_2P to 149.9 eV for CoRuP, as indicated by the dashed lines in Figure 5. This suggests a change in the electronic structure of the compound after the substitution of Ru with Co, specifically an electron transfer/redistribution from phosphorous to ruthenium. Similar binding energy shifts are observed for the other bimetallic compounds, where the binding energy difference is 150.4 and 150.3 eV for MoRuP and NiRuP, respectively. The shift of Ru 3d to lower binding energy is ca. 0.1 eV for RuMoP compared to that of Ru_2P and ca. 0.4 eV for both RuCoP and RuNiP, indicative of a stronger effect of Co and Ni on the electronic structure of Ru compared to that of Mo.

The Ru_2P-type structure has two types of metal sites: tetrahedral (T_d) and square pyramidal (P_y) (Figure 1C). Since the type and structure of the active sites can strongly influence the electrocatalytic activity, calculations were done to determine the type of sites occupied by Co, Ni, and Mo in the bimetallic MRuP structures. The results show that these metals exhibit strong site preference. Specifically, the CoRuP and NiRuP structures are energetically stabilized when all the Co or Ni atoms occupy the T_d sites, and the Ru atoms are in P_y sites (Figure S8A,B). On the contrary, MoRuP is stabilized when Mo is located on the P_y sites while Ru occupies the T_d centers (Figure S8C). Furthermore, XRD patterns were calculated for the possible structures where metals occupy different sites and compared with the experimental ones to further corroborate the thermodynamics stability data. It turns out that for CoRuP and NiRuP, the calculated XRD patterns match the experimental ones only if Co and Ni atoms occupy all tetrahedral sites and Ru atoms occupy all pyramidal sites (Figure S9A–D). In contrast, in the case of MoRuP, the calculated XRD and the experimental patterns match when all Mo atoms occupy the pyramidal sites and Ru atoms occupy the tetrahedral sites (Figure S9E,F).

To gain further understanding of the intrinsic electronic effects responsible for the different performances, DFT calculations were conducted to acquire the partial density of states (PDOS) for the studied catalysts. As shown in Figure 6, replacing Ru with Mo has little effect on the d-band position of the Ru atoms. As a result, the calculated d-band center (ε_d) for Ru of MoRuP is similar to that of Ru_2P (Figure 6), suggesting similar reaction activity, in agreement with the experimental observations. In contrast, substituting Ru with Co or Ni

26379368, 2024, 9, Downloaded from https://onlinelibrary.wiley.com/doi/10.1002/cey2.556 by Humboldt-Universitat Zu Berlin, Wiley Online Library on [06/01/2025]. See the Terms and Conditions (https://onlinelibrary.wiley.com/terms-and-conditions) on Wiley Online Library for rules of use; OA articles are governed by the applicable Creative Commons License

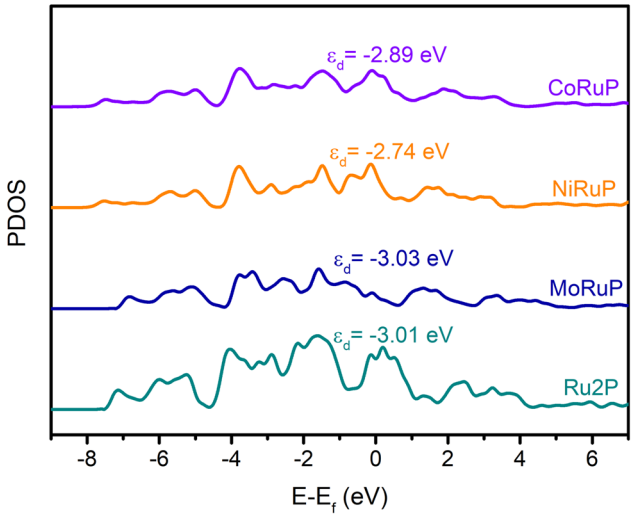

FIGURE 6 DFT calculated PDOS of d-bands and d-band centers ε_d of ruthenium atoms for Ru_2P (cyan), MoRuP (blue), NiRuP(orange), and CoRuP (purple).

can push the positions of the d-bands of the Ru atoms significantly closer to the Fermi level (Figure 6). This kind of shift suggests improved adsorption energy of the intermediates, rationalizing the observed enhanced reaction activity of the CoRuP and NiRuP materials. The trend in the d-band center is consistent with the trend in the XPS Ru 3d shifts observed. Changing the site preference of the metals in the structure leads to a different trend in the calculated ε_d, inconsistent with the experimental observations.

Replacing Ru with Co or Ni, that is, reducing the Ru content, resulted in superior electrochemical performance in acidic and alkaline media, manifested in smaller overpotentials, efficient reaction kinetics, higher TOFs, and mass activities. These findings correlate with the charge redistribution observed via XPS measurements and with the d-band center shift found by DFT calculations. Therefore, based on these findings, we can conclude that the orthorhombic Ru_2P structure represents a suitable matrix for achieving synergism between Ru in P_y sites and Co or Ni in T_d sites, thus offering an effective strategy to derive efficient catalysts while simultaneously reducing the noble metal content.

Owing to the exceptional HER performance of CoRuP in both acidic and alkaline media, Co-containing catalysts were selected for evaluating the effect of further decreasing the Ru content on the HER activity. An additional advantage of the $Co_{2-x}Ru_xP$ catalysts is that since Co_2P crystallizes with the same structure as Ru_2P, the Ru content in the structure can be decreased down to $x = 0$ without structural changes occurring. This means that a clear correlation between the metal composition and HER activity can be established, excluding the effects of structural modifications, which can strongly influence the activity. As the Ru amount gradually decreases in the $Co_{2-x}Ru_xP$ catalysts, the unit cell contracts, and the diffraction peaks continuously shift to higher angles, approaching those of Co_2P (Figure 1B). Solid solutions are therefore achieved over the entire Ru composition range studied (Tables S1 and S2). By decreasing the Ru content to make the Ru/Co ratios be well smaller than 1, the Co atoms will necessarily occupy pyramidal sites in the structure in increasingly higher proportions.

The HER activity slowly declines with decreasing Ru content, although not as much as it would be expected if it was only dependent on the Ru amount in the catalyst (Figure 3), suggesting that the electronic effect of Co over Ru in the P_y sites compensates up to a certain point the replacement of Ru from the T_d of the structure. Therefore, the differences between η_{10} ($\Delta\eta_{10}$) of $Co_{1.9}Ru_{0.1}P$ and Ru_2P are only 26 and 10 mV in H_2SO_4 and KOH, respectively. By contrast, $\Delta\eta_{10}$ values between Co_2P and $Co_{1.9}Ru_{0.1}P$ are 120 and 200 mV, respectively (Figure 3). Clearly, the combination of only a very small amount of Ru (Ru/Co = 0.05) with Co leads to a major activity improvement in comparison with Co_2P. Moreover, despite the activity gradually decreasing as the Ru content is reduced, the losses are not drastic. For example, $Co_{1.5}Ru_{0.5}P$, which has a small Ru/Co ratio of 0.3, performs similarly to Ru_2P in acidic solution and better in basic solution, which still makes it one of the best catalysts reported so far. The catalysts remain highly active up to a Ru/Co ratio of just 0.05, which can be confirmed by comparing them with recently reported catalysts based on Co and Ru phosphides, as they consistently outperform catalysts with similar or higher Ru/Co ratios, as well as those supported on high surface area supports (Table S3), but they are made of amorphous materials or a combination of different Co and Ru phosphides, highlighting the importance of the structure in improving the activity.[12,13,28,29]

The reaction kinetics becomes gradually more sluggish at low pH as the Ru/Co ratio decreases, although not getting close to Co_2P, but remains very fast at high pH, with the Tafel slope remaining close to 30 mV dec^{-1} for $Co_{1.9}Ru_{0.1}P$ (Figure 3F). The enhanced mass activity of the catalysts is maintained in acidic solution even as the Ru/Co ratio is further decreased in the structure to 0.3 and 0.1 in alkaline medium. Although the TOF decreases with decreasing Ru content, it remains significantly higher than that of Pt/C in alkaline solution, even for the sample with the lowest Ru/Co ratio (Figure 4C). Moreover, the intrinsic activities of $Co_{1.5}Ru_{0.5}P$ and $Co_{1.8}Ru_{0.2}P$ remain higher than that of Ru_2P, while that of $Co_{1.9}Ru_{0.1}P$ remains comparable to the activity of Ru_2P and considerably higher than that of

26379368, 2024, 9, Downloaded from https://onlinelibrary.wiley.com/doi/10.1002/cey2.556 by Humboldt-Universitat Zu Berlin, Wiley Online Library on [06/01/2025]. See the Terms and Conditions (https://onlinelibrary.wiley.com/terms-and-conditions) on Wiley Online Library for rules of use; OA articles are governed by the applicable Creative Commons License

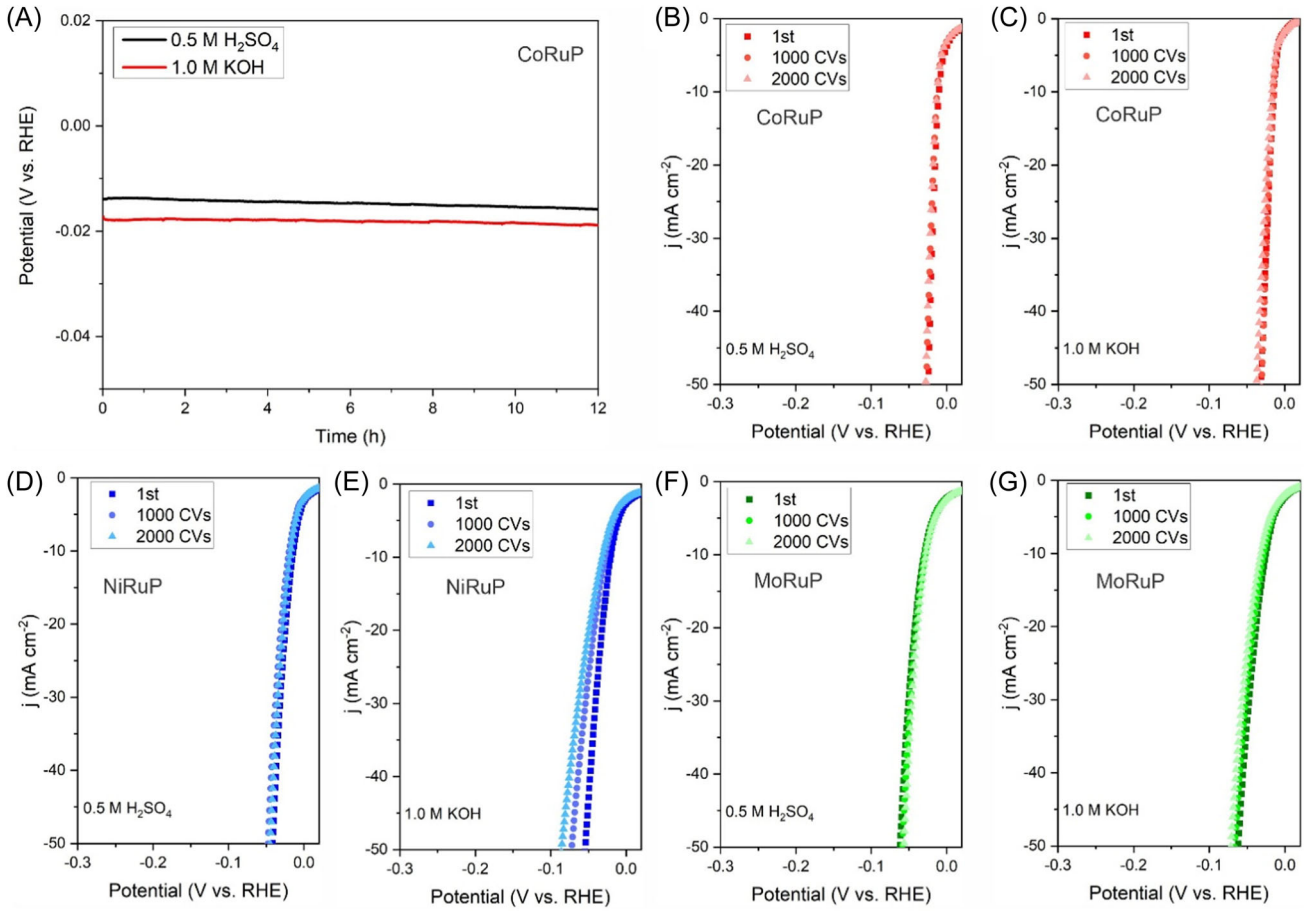

FIGURE 7 (A) Chronopotentiometry curves of the CoRuP catalyst at a constant current density of $-10\ mA\ cm^{-2}$ in 0.5 M H_2SO_4 and 1.0 M KOH. HER polarization curves after 1000 and 2000 CVs of accelerated stability tests of (B, C) CoRuP, (D, E) NiRuP, and (F, G) MoRuP in (B, D, F) 0.5 M H_2SO_4 and (C, E, G) 1.0 M KOH.

Co_2P, which has a relatively lower intrinsic activity. Thus, even a small percentage of Ru combined with Co in the Ru_2P-type structure has a drastic enhancement in the intrinsic activity compared to Co_2P.

Finally, the stability of the catalysts was also evaluated through chronopotentiometry at $-10\ mA\ cm^{-2}$ and CV cycling (Figure 7). CoRuP is stable in both acidic and alkaline solutions, showing negligible decay after 12 h of continuous electrolysis and after 2000 accelerated CV cycles. MoRuP is also fairly stable, while NiRuP shows slight activity attenuation in alkaline medium after 2000 CV cycles. TEM analysis for the post-HER CoRuP catalyst in acidic and alkaline media revealed that the morphology is maintained (Figures S10 and S11). Moreover, EDS mappings showed that the incorporation of Co, Ru, and P is preserved, further emphasizing the stability of the structure. The corresponding HRTEM images, as well as SAED patterns, showed that the CoRuP crystal structure did not change, as inferred from the well-resolved lattice fringes and diffraction rings in the SAED patterns, which match the ones of the pristine CoRuP. Additionally, XPS analysis for the post-HER material in an acidic medium showed negligible changes in the surface (Figure S12), further indicating that $Co_{2-x}Ru_xP$ exhibits not only excellent performance but also good long-term stability.

3 | CONCLUSION

In conclusion, we have developed a facile strategy to synthesize bimetallic Ru-based nanocrystalline phosphides adopting the orthorhombic Ru_2P crystal structure ($M_{2x-1}Ru_xP$, with M = Co, Ni, Mo). Our synthesis approach, which utilized metal phosphonates as precursors, guaranteed homogenous distributions of the elements and the formation of solid solutions. The metals showed site preference in the phosphide structure, with Co and Ni preferring the tetrahedral sites while Ru occupied the pyramidal sites, and Mo preferring the pyramidal sites in MoRuP. The site preference of Co and Ni resulted in a beneficial modulation of the electronic structure of Ru, increasing

26379368, 2024, 9, Downloaded from https://onlinelibrary.wiley.com/doi/10.1002/cey2.556 by Humboldt-Universitat Zu Berlin, Wiley Online Library on [06/01/2025]. See the Terms and Conditions (https://onlinelibrary.wiley.com/terms-and-conditions) on Wiley Online Library for rules of use; OA articles are governed by the applicable Creative Commons License

the d-band center, according to DFT calculations. CoRuP showed the highest HER activity, followed by NiRuP and MoRuP. In acidic medium, CoRuP supported $-10\ mA\ cm^{-2}$ at 12.3 mV (the same as Pt/C) and outperformed Ru_2P. In alkaline medium, CoRuP is also extremely active ($\eta_{10} = 12.9$ mV), with a TOF 10x that of Pt/C. The flexibility of the Ru_2P system to accommodate Co allowed to investigate the impact of the Co percentage on the HER activity. Interestingly, increasing the Co content up to 95 at.% ($Co_{1.9}Ru_{0.1}P$) did not induce drastic activity attenuation, with the catalyst still showing higher TOF than Pt/C and comparable to Ru_2P in the alkaline medium.

4 | EXPERIMENTAL SECTION

4.1 | Materials

N-(phosphonomethyl)iminodiacetic acid (95%), ruthenium chloride hydrate ($RuCl_3{\cdot}xH_2O$), ammonium hydroxide (NH_4OH) solution (30%), and Nafion perfluorinated resin solution (5 wt%) were purchased from Sigma-Aldrich. Anhydrous molybdenum chloride ($MoCl_5$) (99.6%) was purchased from ABCR. 1.0 N H_2SO_4 and 1.0 N KOH solutions for electrochemical measurements, and nickel chloride hexahydrate ($NiCl_2{\cdot}6H_2O$) were purchased from Carl Roth. Absolute ethanol for synthesis was purchased from VWR GmbH. Water with a resistivity of $18.5\ M\Omega\ cm^{-1}$ was used in all syntheses. All chemicals were used as received without further purification.

4.2 | Ru-based phosphonate precursors synthesis

In a typical RuCo-phosphonate synthesis, 0.216 mmol (0.0447 g) of $RuCl_3{\cdot}xH_2O$ was dissolved in 8 mL ethanol in an ultrasound bath. 0.234 mmol (0.0556 g) of $CoCl_2{\cdot}6H_2O$ was dissolved in 5 mL ethanol, added to the Ru-solution, and stirred for 5 min. In a separate vial, 0.25 mmol (0.057 g) of *N*-(phosphonomethyl)iminodiacetic acid was dissolved in 9 mL water, and the pH was adjusted to 3–4 with the addition of 10% NH_4OH solution. 9 mL of ethanol was added to the phosphonic acid solution immediately before the addition of the metal solution. The metal solution was added dropwise to the phosphonic acid solution under stirring (1000 rpm), and the mixture was kept stirring for 30 min, followed by adjustment of the pH to 4 with 10% NH_4OH solution (pH was not allowed to exceed 4.5). The pH was monitored for 1 h and kept at 4 using diluted NH_4OH solution, and the mixture was further stirred for 18 h while maintaining the pH at 4. The product was collected by centrifugation, washed twice with 30 mL ethanol, and dried under air at 70°C overnight. The RuNi- and RuMo-phosphonates were synthesized following the same protocol, except that $CoCl_2{\cdot}6H_2O$ was replaced with $NiCl_2{\cdot}6H_2O$ or $MoCl_5$, respectively, using the same molar ratios. Pristine Co_2P was synthesized using the same approach, using 0.45 mmol of $CoCl_2{\cdot}6H_2O$ as the sole metal. To obtain pure-phase Ru_2P, 0.6 mmol of $RuCl_3{\cdot}xH_2O$ was employed as the sole metal source.

4.3 | Ru-based phosphide synthesis

The phosphides were obtained in one step by pyrolysis of the corresponding phosphonates precursors under H_2(5%)/Ar mixture at 500–700°C. In a typical synthesis, 50 mg of the precursor was placed in a ceramic boat, which was positioned in the center of a tubular furnace (Nabertherm), followed by purging with H_2(5%)/Ar for 20 min before heating. Afterward, the precursor was heated (with a heating ramp of $5.6°C\ min^{-1}$) at the desired temperature for 3 h. The sample was then left to cool down naturally to room temperature, followed by collection and grinding for further work.

4.4 | Characterization

XRD patterns were acquired using an STOE MP diffractometer in transmission mode using Mo Kα radiation ($\lambda = 0.07093$ nm). TEM and HRTEM micrographs were measured on an FEI Talos F200S scanning transmission electron microscope operated at 200 kV. Elemental ratios were determined using ICP-OES (Spectroblue OEB; Ametek) after dissolving the corresponding catalysts in a mixture of concentrated HCl and HNO_3. XPS spectra were acquired in an ultrahigh vacuum chamber with a base pressure of 10^{-9} mbar, using an Al X-ray source ($h\nu = 1486.6$ eV) for excitation. The number of photoelectrons as a function of their kinetic energy was measured using an Omicron EA125 hemispherical analyzer, using pass energies of 50 eV for the survey spectra and 20 eV for the detail scans. The powders were thinly and evenly spread on carbon tape. The binding energy scale of the spectrometer was calibrated by setting the Au $4f_{7/2}$ peak of an Au(111) reference sample to 84.0 eV. Since some samples exhibited charging, we set the carbon C–C peak of the carbon tape to 285.0 eV as the reference.

4.5 | Electrochemical measurements

Electrochemical measurements were acquired using a Bio-Logic VMP3 potentiostat/galvanostat equipped

26379368, 2024, 9, Downloaded from https://onlinelibrary.wiley.com/doi/10.1002/cey2.556 by Humboldt-Universitat Zu Berlin, Wiley Online Library on [06/01/2025]. See the Terms and Conditions (https://onlinelibrary.wiley.com/terms-and-conditions) on Wiley Online Library for rules of use; OA articles are governed by the applicable Creative Commons License

with a built-in electrochemical impedance spectroscopy (EIS) analyzer. The HER of the catalysts was measured in a three-electrode electrochemical cell using a 3 mm diameter GC rotating disc electrode (RDE). RHE (Gaskatel) and carbon paper were employed as reference electrode and counter electrode, respectively. The catalysts' inks were prepared as follows: 3 mg of the catalyst and 1 mg of carbon super P were added to 470 μL 1:1 water/ethanol and 30 μL of 5 wt% Nafion solution, and the mixture was sonicated for ca. 30 min to obtain a homogeneous ink. The electrodes were prepared by drop casting 3 μL of the catalyst ink onto the GC disc and drying at room temperature to achieve a loading of 0.25 mg cm^{-2}. Before catalyst casting, the GC electrode was polished with several grades of alumina slurry of 1 and 0.05 μm sequentially and then rinsed with deionized water and dried in air. The HER measurements were carried out in 0.5 M H_2SO_4 and 1.0 M KOH solutions at 25°C with the RDE rotated at 2000 rpm. CV experiments were performed in the potential window −0.1 to 0.03 V versus RHE with a scan rate of 20 mV s^{-1}. Linear sweep voltammetry (LSV) curves were measured in the potential window −0.25 to 0.05 V versus RHE with a scan rate of 5 mV s^{-1}. All represented polarization curves were corrected against iR-drop, where solution/ohmic resistance was determined with EIS measurements. The accelerated CV stability tests were conducted using RDE setup by sweeping the potential between −0.08 and 0.02 V at a scan rate of 100 mV s^{-1} for 2000 CVs, followed by measuring LSV between −0.25 to 0.05 V at 5 mV s^{-1}. The chronopotentiometric curves were measured using carbon paper as a support at −10 mA cm^{-2} for 10 h.

The TOF values were calculated for each catalyst according to the following equation:

$$\mathrm{TOF} = \frac{j \times A}{2nF}, \tag{1}$$

where j is the current density (A cm^{-2}), A is the geometric surface area (cm^{-2}), F is the Faraday constant (96,500 C mol^{-1}), and n is the number of active sites. The number of active sites was determined experimentally using the protocol devised by Hu et al.,[18,27] employing the CV technique. All CVs were recorded in phosphate buffer solution (pH 7) in the potential window 0.0–0.6 versus RHE at 50 mV s^{-1} scan rate. The surface charge (Q), which is proportional to the number of active sites, was then calculated to be half of the whole charge integrated over the entire CV for each catalyst (Figure S5). Thus, the number of active sites $n = Q/F$ (moles).

4.6 | Computational models and method

All the electronic structure calculations were performed using the plane-wave periodic DFT as implemented in the Vienna ab initio simulation package.[30–32] The projector augmented-wave method developed by Blöchl to describe the electron-ion interactions using plane wave basis sets was employed.[33] The generalized gradient approximation with the Perdew–Burke–Ernzerh exchange-correlation functional was used.[34] The kinetic energy cutoff was set to 700 eV. The convergence criteria for the energy calculations were set to a self-consistent field tolerance of 1.0×10^{-8} eV. All internal structure parameters were relaxed until the maximum Hellmann–Feynman force on each ion was less than 0.003 eV $Å^{-1}$. Integration over the Brillouin zone was achieved using a k-points mesh of $6 \times 5 \times 4$ according to the Monkhorst–Pak scheme.[35] The powder XRD patterns of the structures obtained by energy minimization as described above have been calculated using the VESTA3 software,[36] which utilizes RIETAN-FP[37] to simulate X-ray and neutron powder diffraction patterns from lattice and structure parameters. The d-band center (ε_d) was calculated using the following equation:

$$\varepsilon_d = \frac{\int_{-\infty}^{E_f} E\rho_d(E)dE}{\int_{-\infty}^{E_f} \rho_d(E)dE}, \tag{2}$$

where ρ_d represents the density of states projected onto the target metal's d band and E_f is the Fermi energy.[38]

ACKNOWLEDGMENTS

The authors thank C. Erdmann for the transmission electron microscopy measurements.

CONFLICT OF INTEREST STATEMENT

The authors declare that there are no conflicts of interests.

DATA AVAILABILITY STATEMENT

Data that support the findings of this study are available from the corresponding authors upon reasonable request.

ORCID

Patrícia A. Russo https://orcid.org/0000-0002-1082-2302
Thorsten Schultz https://orcid.org/0000-0002-0344-6302
Zhe-Ning Chen https://orcid.org/0000-0003-3821-5843
Norbert Koch https://orcid.org/0000-0002-6042-6447
Nicola Pinna http://orcid.org/0000-0003-1273-803X

26379368, 2024, 9, Downloaded from https://onlinelibrary.wiley.com/doi/10.1002/cey2.556 by Humboldt-Universitat Zu Berlin, Wiley Online Library on [06/01/2025]. See the Terms and Conditions (https://onlinelibrary.wiley.com/terms-and-conditions) on Wiley Online Library for rules of use; OA articles are governed by the applicable Creative Commons License

REFERENCES

1. Roger I, Shipman MA, Symes MD. Earth-abundant catalysts for electrochemical and photoelectrochemical water splitting. *Nat Rev Chem*. 2017;1(1):0003.
2. Seh ZW, Kibsgaard J, Dickens CF, Chorkendorff I, Nørskov JK, Jaramillo TF. Combining theory and experiment in electrocatalysis: insights into materials design. *Science*. 2017;355(6321):eaad4998.
3. Wang H, Liu X, Niu P, Wang S, Shi J, Li L. Porous two-dimensional materials for photocatalytic and electrocatalytic applications. *Matter*. 2020;2(6):1377-1413.
4. Zhu J, Hu L, Zhao P, Lee LYS, Wong K-Y. Recent advances in electrocatalytic hydrogen evolution using nanoparticles. *Chem Rev*. 2020;120(2):851-918.
5. El-Refaei SM, Russo PA, Pinna N. Recent advances in multimetal and doped transition-metal phosphides for the hydrogen evolution reaction at different pH values. *ACS Appl Mater Interfaces*. 2021;13(19):22077-22097.
6. Danilovic N, Subbaraman R, Strmcnik D, et al. Enhancing the alkaline hydrogen evolution reaction activity through the bifunctionality of $Ni(OH)_2$/metal catalysts. *Angew Chem Int Ed*. 2012;51(50):12495-12498.
7. Mitchell WJ, Xie J, Jachimowski TA, Weinberg WH. Carbon monoxide hydrogenation on the Ru(001) surface at low temperature using gas-phase atomic hydrogen: spectroscopic evidence for the carbonyl insertion mechanism on a transition metal surface. *J Am Chem Soc*. 1995;117(9):2606-2617.
8. Liu Y, Li X, Zhang Q, et al. A general route to prepare low-ruthenium-content bimetallic electrocatalysts for pH-universal hydrogen evolution reaction by using carbon quantum dots. *Angew Chem Int Ed*. 2020;59(4):1718-1726.
9. Zheng Y, Jiao Y, Zhu Y, et al. High electrocatalytic hydrogen evolution activity of an anomalous ruthenium catalyst. *J Am Chem Soc*. 2016;138(49):16174-16181.
10. Yu J, He Q, Yang G, Zhou W, Shao Z, Ni M. Recent advances and prospective in ruthenium-based materials for electrochemical water splitting. *ACS Catal*. 2019;9(11):9973-10011.
11. Luo W, Wang Y, Cheng C. Ru-based electrocatalysts for hydrogen evolution reaction: recent research advances and perspectives. *Mater Today Phys*. 2020;15:100274.
12. Li W, Zhao Y, Liu Y, et al. Exploiting Ru-induced lattice strain in CoRu nanoalloys for robust bifunctional hydrogen production. *Angew Chem Int Ed*. 2021;60(6):3290-3298.
13. Zhang F, Zhu Y, Chen Y, et al. RuCo alloy bimodal nanoparticles embedded in N-doped carbon: a superior pH-universal electrocatalyst outperforms benchmark Pt for the hydrogen evolution reaction. *J Mater Chem A*. 2020;8(25):12810-12820.
14. Tu K, Tranca D, Rodríguez-Hernández F, et al. A novel heterostructure based on RuMo nanoalloys and N-doped carbon as an efficient electrocatalyst for the hydrogen evolution reaction. *Adv Mater*. 2020;32(46):2005433.
15. Liu T, Wang J, Zhong C, et al. Benchmarking three ruthenium phosphide phases for electrocatalysis of the hydrogen evolution reaction: experimental and theoretical insights. *Chem Eur J*. 2019;25(33):7826-7830.
16. Li G, Xu Y, Song Z, et al. Obstructed surface states as the descriptor for predicting catalytic active sites in inorganic crystalline materials. *Adv Mater*. 2022;34(26):2201328.
17. Kim J-C, Lee CW, Kim D-W. Dynamic evolution of a hydroxylated layer in ruthenium phosphide electrocatalysts for an alkaline hydrogen evolution reaction. *J Mater Chem A*. 2020;8(11):5655-5662.
18. Xu J, Liu T, Li J, et al. Boosting the hydrogen evolution performance of ruthenium clusters through synergistic coupling with cobalt phosphide. *Energy Environ Sci*. 2018;11(7):1819-1827.
19. Yang B, Xu J, Bin D, et al. Amorphous phosphatized ruthenium–iron bimetallic nanoclusters with pt-like activity for hydrogen evolution reaction. *Appl Catal B*. 2021;283:119583.
20. Wong-Ng W, Ching WY, Xu Y-N, Kaduk JA, Shirotani I, Swartzendruber L. Structure and electronic properties of the orthorhombic MoRuP superconductor prepared at high pressure. *Phys Rev B*. 2003;67(14):144523.
21. Ohta S. Magnetic properties of 4d metal phosphides containing Co and Ni. *J Phys Soc Jpn*. 1996;65(12):4090-4091.
22. Zhang R, Russo PA, Feist M, Amsalem P, Koch N, Pinna N. Synthesis of nickel phosphide electrocatalysts from hybrid metal phosphonates. *ACS Appl Mater Interfaces*. 2017;9(16):14013-14022.
23. El-Refaei SM, Russo PA, Amsalem P, Koch N, Pinna N. The importance of ligand selection on the formation of metal phosphonate-derived CoMoP and $CoMoP_2$ nanoparticles for catalytic hydrogen evolution. *ACS Appl Nano Mater*. 2020;3(5):4147-4156.
24. Liu T, Wang S, Zhang Q, Chen L, Hu W, Li CM. Ultrasmall Ru_2P nanoparticles on graphene: a highly efficient hydrogen evolution reaction electrocatalyst in both acidic and alkaline media. *Chem Commun*. 2018;54(27):3343-3346.
25. Strmcnik D, Lopes PP, Genorio B, Stamenkovic VR, Markovic NM. Design principles for hydrogen evolution reaction catalyst materials. *Nano Energy*. 2016;29:29-36.
26. Wu M-Y, Da P-F, Zhang T, Mao J, Liu H, Ling T. Designing hybrid NiP_2/NiO nanorod arrays for efficient alkaline hydrogen evolution. *ACS Appl Mater Interfaces*. 2018;10(21):17896-17902.
27. Merki D, Fierro S, Vrubel H, Hu X. Amorphous molybdenum sulfide films as catalysts for electrochemical hydrogen production in water. *Chem Sci*. 2011;2(7):1262-1267.
28. Zhu T, Huang J, Huang B, et al. Huang high-index faceted RuCo nanoscrews for water electrosplitting. *Adv Energy Mater*. 2020;10(47):2002860.
29. Wang C, Wang Y, Shi Z, et al. RuCo alloy nanoparticles embedded into N-doped carbon for high efficiency hydrogen evolution electrocatalyst. *Energies*. 2022;15(8):2908.
30. Kresse G, Furthmüller J. Efficient iterative schemes for ab initio total-energy calculations using a plane-wave basis set. *Phys Rev B*. 1996;54(16):11169-11186.
31. Kresse G, Furthmüller J. Efficiency of ab-initio total energy calculations for metals and semiconductors using a plane-wave basis set. *Comput Mater Sci*. 1996;6(1):15-50.
32. Kresse G, Hafner J. Ab initio molecular dynamics for open-shell transition metals. *Phys Rev B*. 1993;48(17):13115-13118.
33. Blöchl PE. Projector augmented-wave method. *Phys Rev B*. 1994;50(24):17953-17979.
34. Perdew JP, Burke K, Ernzerhof M. Generalized gradient approximation made simple. *Phys Rev Lett*. 1996;77(18):3865-3868.
35. Van Der Sluis P, Spek AL. BYPASS: an effective method for the refinement of crystal structures containing disordered solvent regions. *Acta Crystallogr A*. 1990;46(3):194-201.

26379368, 2024, 9, Downloaded from https://onlinelibrary.wiley.com/doi/10.1002/cey2.556 by Humboldt-Universitat Zu Berlin, Wiley Online Library on [06/01/2025]. See the Terms and Conditions (https://onlinelibrary.wiley.com/terms-and-conditions) on Wiley Online Library for rules of use; OA articles are governed by the applicable Creative Commons License

36. Momma K, Izumi F. VESTA 3for three-dimensional visualization of crystal, volumetric and morphology data. *J Appl Crystal*. 2011;44(6):1272-1276.
37. Izumi F, Momma K. Three-dimensional visualization in powder diffraction. *Solid State Phenom*. 2007;130:15-20.
38. Hammer B, Nørskov JK. Theoretical surface science and catalysis-calculations and concepts. *Adv Catal*. 2000;45:71-129.

SUPPORTING INFORMATION

Additional supporting information can be found online in the Supporting Information section at the end of this article.

How to cite this article: El-Refaei SM, Russo PA, Schultz T, et al. Activating Ru in the pyramidal sites of Ru_2P-type structures with earth-abundant transition metals for achieving extremely high HER activity while minimizing noble metal content. *Carbon Energy*. 2024;6:e556. doi:10.1002/cey2.556

26379368, 2024, 9, Downloaded from https://onlinelibrary.wiley.com/doi/10.1002/cey2.556 by Humboldt-Universitat Zu Berlin, Wiley Online Library on [06/01/2025]. See the Terms and Conditions (https://onlinelibrary.wiley.com/terms-and-conditions) on Wiley Online Library for rules of use; OA articles are governed by the applicable Creative Commons License